Water Science & Technology

IWA PUBLISHING

Water Science & Technology Vol 87 No 4, 954 doi: 10.2166/wst.2023.025

Hydraulic modeling of a compact stormwater treatment device applying concepts of dynamic similitude

Max Stricker [a,*], Tobias Littfinski[a], Klaus Hans Pecher[b], Manfred Lübken [a] and Marc Wichern [a]

[a] Department of Civil and Environmental Engineering, Institute of Urban Water Management and Environmental Engineering, Ruhr-Universität Bochum, Universitätsstraße 150, Bochum 44801, Germany
[b] Dr. Pecher AG, Klinkerweg 5, Erkrath 40699, Germany
*Corresponding author. E-mail: max.stricker@rub.de

MS, 0000-0003-3306-4441

ABSTRACT

The development of compact treatment devices (CTDs) with high removal efficiencies and low space requirements is a key objective of urban stormwater treatment. Thus, many devices utilize a combination of sedimentation and upward-flow filtration in a single system. Here, sedimentation is used before filtration, which makes it difficult to evaluate the individual treatment stages separately. This study determines the removal efficiency by sedimentation and the expected filter load in a specific compact treatment device designed for a catchment area of up to 10,000 m^2. In contrast to a full-scale investigation, small-scale physical hydraulic modeling is applied as a new cost-saving alternative. To validate upscaling laws, tracer signals and particle-size-specific removal efficiencies are determined for two geometrically similar models at different length scales. Thereby, Reynolds number similarity produces similar flow patterns, while the similarity of Hazen numbers allows to upscale removal efficiencies. Upscaling to the full-scale reveals that the filter in the device is only partly loaded by particulate matter that consists mostly of particles $\leq$63 μm. Thus, sedimentation upstream of a filter is of relevant importance in CTDs. The proposed dimensionless relationship may be used for particles from different catchments and helps to size the device accordingly.

Key words: best management practices, dimensional analysis, hydraulic modeling, sedimentation, stormwater

HIGHLIGHTS

- A small-scale approach is presented to study the gravity-driven removal efficiency in a compact stormwater treatment device that combines sedimentation and filtration.
- The Hazen number is successfully applied to scale the gravity-driven removal of particles from a small- to a full-scale model.
- The filter stage of the device is only partially loaded with particulate matter, which mostly consists of particles $\leq$63 μm.

GRAPHICAL ABSTRACT

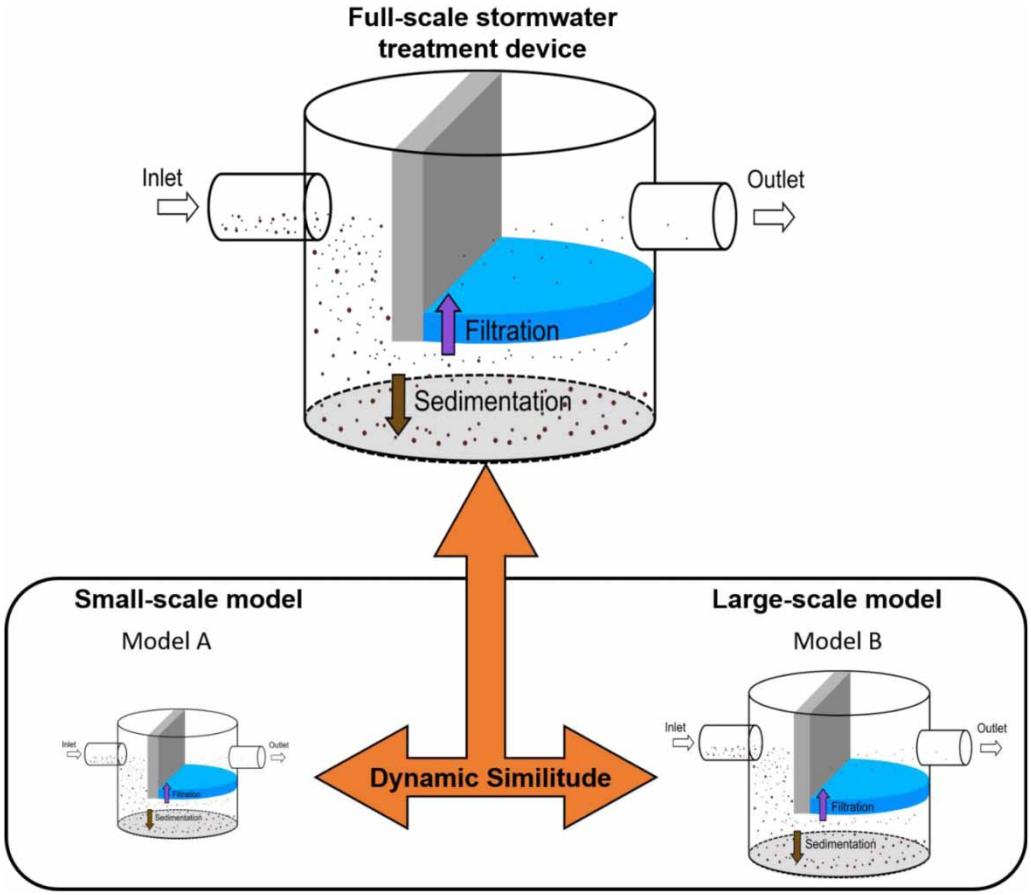

1. INTRODUCTION

Due to increasing knowledge of pollutant pathways, new urban stormwater management practices have been developed in recent decades, which are commonly referred to as best management practices (BMPs), stormwater control measures (SCM) or low impact development (LID) (Fletcher *et al.* 2015). These include compact treatment devices (CTDs) integrated into the underground stormwater sewer system, which treat stormwater in a decentralized or semicentralized manner and are often designed for the treatment of road runoff. Road runoff is known to be heavily polluted with particulate matter and soluble pollutants. Particulate matter is often generated by tire, brake and road wear and consists to a large extent of particles in the spectrum of ≤63 μm (Gelhardt *et al.* 2017). Additionally, the transport of many pollutants can also be attributed to particulate matter, since they are partly present in particle-bound or particulate form (Maniquiz-Redillas & Kim 2014; Huber *et al.* 2016). The retention of fine particulate matter ≤63 μm in CTDs is therefore a decisive criterion for their effectiveness and has recently been defined as a target parameter for stormwater treatment in German worksheets (DWA & BWK 2020). Therefore, some CTDs combine an upstream sedimentation with a filter stage within a single system (CTD-SF) to achieve the highest possible retention of fine particulate matter. The upstream sedimentation stage reduces the filter load and can thus extend the time until the filter clogs (Herr & Sansalone 2015). The lifetime of the filter stage is an important operating cost factor, as it determines the maintenance intervals. Therefore, evaluating the effectiveness of the sedimentation stage in a CTD-SF is critical because it directly affects the filter loading and thus the life of the filter stage. In addition, filtration mechanisms depend on a number of variables, of which the size of the particles in the influent and the grain size of the filter medium play an important role (Kandra *et al.* 2015).

However, there is little information on the different separation mechanisms in CTD-SFs, and most of the investigations have been performed on the less complex CTDs without a filter stage. Existing information on CTDs comes either from

laboratory tests developed and conducted for the purpose of design approval or, less frequently, from *in situ* field studies. While *in situ* studies can provide important information on the retention to be expected in the field, they are often subject to greater measurement uncertainties under highly variable conditions (Langeveld *et al.* 2012; Lieske *et al.* 2021). Full-scale laboratory tests allow testing under controlled conditions. However, they require test rigs with appropriate hydraulic capacity and capabilities for automated metering of larger quantities of test material (Boogaard *et al.* 2015; Neupert *et al.* 2021). Here, too, some uncertainties may still exist due to partial volume sampling of large quantities of volume flow (Dufresne *et al.* 2010; Neupert *et al.* 2021). Some devices (CTDs and CTD-SFs) on the market are designed for catchment areas of up to 30,000–45,000 m^2 with a maximum hydraulic treatment capacity of roughly 45 to 70 $L\ s^{-1}$, respectively (Sommer *et al.* 2015). The volume of filter substrate used in CTD-SFs can range from about 0.4 to 0.03 $L\ m^{-2}$ catchment area depending on the device (Grüning & Schmitz 2018). For CTD-SFs, the investigation of sedimentation efficiency is particularly challenging, since it requires a representative measurement upstream of the filter stage or access to the sedimentation chamber. In addition, it can generally be assumed that the flow resistance of the filter stage influences the flow through the upstream sedimentation chamber (Stricker *et al.* 2022). Therefore, the effectiveness of the sedimentation chamber cannot be accurately assessed without the presence of the filter stage. To date, there are no full-scale laboratory studies on the effectiveness of a sedimentation stage in CTD-SFs. Studies based on *in situ* measured data on the effectiveness of the sedimentation stage in CTD-SFs have previously been conducted on smaller systems with catchment areas of 500 and 1,000 m^2 (Herr & Sansalone 2015; Liu & Sansalone 2019). Herein, the authors found that over an operating period of more than one year, 77 and 87% of the particulate matter was retained in the sedimentation stage. A single *in situ* study investigated a CTD-SF connected to a catchment area of 10,000 m^2. Thereby, a 71% removal was calculated by a mass balance derived by drawing samples from the influent, the effluent and below the filter bed (Wichern *et al.* 2017). In addition to the challenge of transferring *in situ* results to other sites (Spelman & Sansalone 2018), it is uncertain to what extent efficiencies can be transferred to other system types: all CTDs and CTD-SFs are industrial products of different manufacturers and therefore vary in size and type. Furthermore, it is unclear how and whether basic principles of existing dimensioning recommendations of rectangular sedimentation basins can be used for the general dimensioning of these systems. Rectangular sedimentation basins are usually sized on the basis of surface loading rate (EPA 1986; DWA & BWK 2020), which is derived from model concepts of classic sedimentation theories (Hazen 1904; Camp 1946). Therefore, in the context of dimensioning, a uniform horizontal flow in a rectangular basin is often assumed. If applicable to CTD-SFs, these mathematical models of classic sedimentation theory may provide information on the removal efficiency without difficult measurements underneath the filter stage (Herr & Sansalone 2015). However, the flow patterns in CTDs and CTD-SFs are often far from ideal in the sense of the classical sedimentation theory because they are built for much smaller footprints than rectangular basins. Previous studies of CTDs showed that classical mathematical models often need adjustment to the specific device (Boogaard *et al.* 2015; Liu & Sansalone 2019).

The objective of this study is to determine the removal efficiency of particulate matter in the sedimentation stage in a CTD-SF designed for catchment areas up to 10,000 m^2, although in practice the CTD-SF is often connected to smaller catchments. By this, not only the removal of particulate matter in the sedimentation stage but also the filter load can be determined, which allows conclusions on the expected lifetime of the filter stage. However, accessing data from the sedimentation chamber underneath a filter stage remains a difficult task on large full-scale systems. For this reason, this study presents an alternative approach by investigating a CTD-SF by physical hydraulic modeling. Thereby, small-scale physical models are built and tested under laboratory conditions. Usually, the physical models are designed in accordance with the geometric features of the original, i.e. the device in full-scale. Contrary to full-scale investigations, hydraulic physical modeling is cost and time-saving since it significantly reduces the quantity of volume flow to be sampled. Most importantly, it allows direct access to the sedimentation chamber, which is hard to achieve on a full-scale CTD-SF. However, transferring results from small-scale models to the full-scale original demands the investigation of valid upscaling laws. Therefore, the decision to physically model a CTD-SF added a central objective to this study: Is it possible to transfer data of removal efficiency obtained from model tests to the full-scale of a CTD-SF?

Generally, the results of the hydraulic model tests are scaled to the original by applying relationships derived from the principles of dynamic similitude. These relationships are expressed as nondimensional numbers (e.g. Reynolds number) that characterize, by their numerical value, the nature of the flow under consideration. In the field of stormwater treatment, physical hydraulic modeling was used for studies of rectangular sedimentation basins (Thompson 1969; Kawamura 1981; Stovin & Saul 1994; Sekimoto 2008; Takamatsu *et al.* 2010) and for vortex separators (Weiß & Michelbach 1996). The validity of nondimensional numbers can either be checked by comparing the model results to the original or by comparing them to a

geometrically similar model on a different length scale (Emori & Schuring 1977). The latter one benefits from reduced cost and improved accessibility of the involved physical processes, whereas the direct comparison with the full-scale is mostly avoided.

In summary, the objectives of this study are as follows:

(i) Physical hydraulic modeling of the sedimentation process in a compact treatment device with combined sedimentation and filtration and investigation of valid upscaling laws for sedimentation.
(ii) Evaluation of particle-size-specific removal efficiencies of Millisil W4 in the sedimentation stage and testing the applicability of mathematical models of classical sedimentation theory.
(iii) Site-specific prediction of the filter load after preliminary sedimentation for the full-scale.

2. METHODS

2.1. Concept of dynamic similitude

The physical variables of sedimentation in a settling device can be expressed as a set of nondimensional numbers based on the dimensional analysis. Dynamic similarity theory implies that the removal efficiency of particulate matter is a function of applicable nondimensional numbers. This means that the results of physical hydraulic model tests can be transferred to the full-scale of the original if the relevant nondimensional numbers are of the same numerical value in the model and original. However, often not all nondimensional numbers can be kept constant. In this case, it is necessary to investigate the influence of the nondimensional numbers on the physical process. The general concept of dynamic similitude is explained in detail in various basic works (Emori & Schuring 1977; Kobus 1984). It follows from the dimensional analysis that the efficiency η of a settling device is mainly a function of different dimensionless numbers (Hazen 1904; Thompson 1969; Weiß & Michelbach 1996; Li & Sansalone 2021):

$$\eta = f(Re,\ F_r, Ha,\ L_R,\ \ldots, \Pi_i) \tag{1}$$

where the most relevant nondimensional numbers are the Reynolds number (Re), the Froude number (Fr), the Hazen number (Ha) and any ratio of geometric length scales (L_R). Theoretically, other nondimensional numbers Π_i can be formed at will from characteristic quantities of the device. However, the most common nondimensional numbers for sedimentation are the Reynolds number, the Hazen number and the densiometric Froude number, which are defined as follows:

$$Re = \frac{U \cdot L}{\vartheta}, \quad Fr = \frac{U^2 \rho_w}{Lg(\rho_p - \rho_w)} \quad Ha = \frac{v_s}{q_A} \tag{2}$$

In these equations, U is the characteristic velocity (m s^{-1}), L is the characteristic length (m), ρ_w is the density of water (kg m^{-3}), ρ_p is the density of particulate matter (kg m^{-3}), ϑ is the kinematic viscosity (m^2 s^{-1}), v_s is the settling velocity (m s^{-1}), q_A is the surface loading rate (m h^{-1}), which is defined as the ratio of flow rate to the settling area of the device.

The Reynolds number indicates the conditions under which the ratio of viscous forces to inertial forces is the same in both model and original. Moreover, it indicates the transition from laminar to turbulent flow, which greatly influences the inside flow patterns. The densiometric Froude number expresses the condition for the similarity of buoyant and inertia forces. However, Reynolds and Froude similarity spells out conflicting model design requirements (Emori & Schuring 1977). The Hazen number expresses the relation of the settling time scale and the hydraulic retention time scale, which is represented by the surface loading rate (Hazen 1904; Camp 1946). For instance, when the numerical value of the Hazen number is the same in the model and the original, the ratio of settling velocity and surface loading rate is identical. Throughout the literature, the Hazen number is a common nondimensional group used to predict and scale removal efficiencies in settling devices (Hazen 1904; Thompson 1969; Weiß & Michelbach 1996; Takamatsu *et al.* 2010; Li & Sansalone 2021). Moreover, it proved to be a robust nondimensional group for a set of different rectangular basin configuration and loading conditions (Li & Sansalone 2021). However, scaling solely on Hazen number contradicts also with Reynolds similarity, which may lead to an overestimation of removal efficiency when scaling the removal efficiency from the model to the full-scale (Weiß 1997). Thompson (1969) achieved similarity between two rectangular tank geometries of the same model family by scaling with Hazen number. In addition, his study did not show a dependence of Reynolds or Froude number on the removal

efficiency. This however may be due to the fact that the Reynolds number already was above a critical value. Exceeding this value, Thompson (1969) suggests, will diminish the influence of the Reynolds number and can make the flow pattern independent of Reynolds number (Clements *et al.* 1969). This is also indicated by Kobus (1984) who suggests that a relaxation of Reynolds number is tolerable, as long as it exceeds a critical value. Within this constraint, the modeling of gravity-driven flows by Froude similarity may be preferable over Reynolds similarity because it allows maintaining macroscopic turbulent features of the flow while also enabling Froude similarity. This approach was used by Sekimoto (2008) who modeled the removal efficiencies in two differently scaled models of a water-driven sedimentation basin using Froude number, while the Reynolds number in the smaller model still exceeded 20,000. However, by applying just the Froude number similarity between both models, the similarity was not achieved with respect to the removal of small particles (<200 μm), which are of major concern for the treatment of polluted road runoff in separate sewer systems. In this study, scaling laws are verified by comparing two differently scaled physical models of the same CTD-SF to each other (Thompson 1969; Emori & Schuring 1977; Sekimoto 2008).

2.2. Hydraulic modeling of a compact treatment device combining sedimentation and filtration

The device investigated is a compact treatment device combining sedimentation and filtration (FiltaPex® Standard-BE2400, Pecher Technik GmbH, Erkrath Germany) for the treatment of road runoff. The main treatment objectives are the removal of fine particulate matter by a combination of sedimentation and filtration, and the removal of pollutants such as heavy metals and hydrocarbons by filtration and adsorption. Additional information on the filter stage is given in the Supplementary Information (SI). The device is shaft-shaped and designed for installation in a separate sewer system. Principal geometry and functions are outlined in Figure 1. Herein, stormwater enters via the inlet and is deflected downwards by a baffle (gray block, see Figure 1(d)), which is vertically separating the shaft into two sections. In the rear section, a filter stage is implemented (blue semicircle, see Figure 1(d)). Theoretically, the entire base area of the device is available for sedimentation. As the operating time increases, the filter becomes clogged with particles causing a decrease in hydraulic permeability. Thus, depending on rainfall intensity and filter condition, the water level in the first section and in the inlet pipe may increase. The differential water level between the inlet and the outlet (Δh) is generating the driving pressure gradient for the water to percolate through the filter media. When the upstream water level exceeds the height of the baffle, the water short-circuits the filter media and is discharged over the baffle exiting through the outlet. In general, the lifetime of the filter media ends when the designed value of volume flow is not able to pass the filter stage due to an increased pressure drop over the filter stage. The

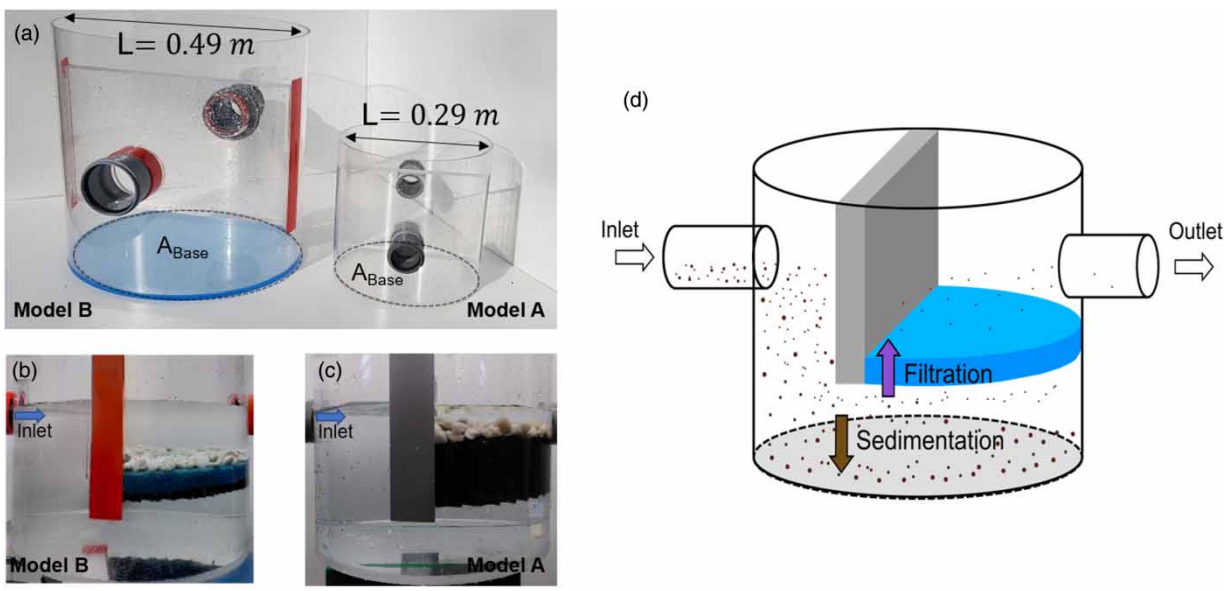

Figure 1 | Physical hydraulic models: (a) model A (right) and model B (left) without filter stage. (b) model B and (c) model A with filter stage under experimental conditions. (d) Functional scheme of the compact treatment device combining sedimentation and filtration.

full-scale device has a shaft diameter of 2.4 m, 2.5 m^2 of filter area and is meant to treat runoff for catchment areas up to 10,000 m^2. Detailed information on the geometry is given in the SI in Figure S1.

In this study, two physical hydraulic models of the full-scale CTD-SF under investigation were built at different scales. Herein the small model (model A) and the large model (model B) are built with shaft diameters of 0.29 and 0.49 m, respectively. Since the full-scale device has a diameter of $L = 2.4$ m, the ratio of length scales is 1:8.3 for model A and 1:4.9 for model B. All other geometric features were scaled using these ratios. Both models are depicted in Figure 1(a). Since the aim of this study is to investigate the removal efficiency by sedimentation, the modeling of the filter stage was relaxed to some extent. Therefore, the only property of the filter stage in the full-scale device that is considered in the models is its ability to balance the flow along the filter surface by providing flow resistance and thereby affecting the flow pattern in the sedimentation chamber. Modeling any internal processes of the filter stage in this setup was discarded and is best done in a standalone experiment. To include filter resistance in the model, filter mats from aquarium supplies (Pondlife Hanako Koi, Germany) were used. These have an open foam structure with 30 PPI (pores per inch). The thickness of the filter mats in model B corresponds to 3 cm. To provide some additional resistance to the higher momentum in model A, the thickness was doubled in model A to 6 cm. The filter mats were placed on a filter media support (12 × 12 mm). To prevent the filter mats from lifting, they were weighted with coarse gravel ($d = 25$–40 mm), see Figure 1(b) and 1(c).

Four assumptions were used to further reduce complexity of the models: (i) a condition of the full-scale CTD-SF is investigated in which the pressure drop by the filter, i.e. water column height in front of the baffle (Δh) is negligibly small in comparison with other geometric length scales. This condition can be expected for the full-scale device at low particulate filter load and/or low volumetric flow rates and allows to achieve the geometric similarity between models and CTD-SF as long as the observed water column height goes towards zero ($\Delta h \to 0$). This assumption holds true for both models A and B, since the water column height in front of the baffle is negligible small under experimental conditions, see Figure 1(b) and 1(c). (ii) Secondly, it is assumed that the filter stage is isotropic, i.e. the filter permeability and thus the pressure drop across the filter depth is the same at any location. (iii) Thirdly, steady-state conditions, i.e. constant inflow and outflow rates are investigated. (iv) Fourth, it is assumed that the flow pattern in the sedimentation chamber is relatively insensitive to the magnitude of the filter resistance as long as a filter is present.

The full-scale CTD-SF is modeled for a rainfall intensity of 2.9 L s^{-1} ha^{-1}. At this condition, the flow in the inlet pipe is already in the turbulent regime ($Re_{hyd} \approx 9{,}000$–$19{,}000$). Initial considerations to take the Hazen or Froude number for the modeling were therefore discarded since this would have meant losing the turbulent properties in the inflow. Thereby, the physical models would have been operated at hydraulic Reynolds numbers in the range of 130–900 depending on model scale and water level in the inlet pipe. Thus, Reynolds number was used to produce a similar flow pattern and maintain turbulent features both in the models and the full-scale device. Reynolds similarity is achieved by adjusting the volume flow rates Q_i in the models (Kobus 1984):

$$\frac{Q_i}{Q_{\text{Full-scale}}} = \frac{L_i}{L_{\text{Full-scale}}} \tag{3}$$

where Q_i (m^3 s^{-1}) is the influent and effluent flow rate in the models for $i = A$ or B; L_i (m) the characteristic length scale, i.e. the shaft diameter of the models A or B; $L_{\text{Full-scale}}$ (m) is the shaft diameter of the full-scale device. The adjustment of the volume flow rates leads to different properties of the models, which are summarized in Table 1. Note that control

Table 1 | Properties of the models and the full-scale device at Reynolds similarity

	Model A	Model B	Full-scale device
Diameter L (m)	0.29	0.49	2.4
Rainfall intensity r (L s^{-1} ha^{-1})	–	–	2.9
Volume flow rate Q (m^3 h^{-1})	1.28 ± 0.025	2.14 ± 0.032	10.48
Base area A_{Base} (m^2)	0.066	0.189	4.52
Surface loading rate q_A (m h^{-1})	19.36 ± 0.378	11.32 ± 0.169	2.32
Tracer volume V_{Tracer} (mL)	35	100	–

measurements of the volume flow rates revealed a small systematic error in model A. Herein, the volume flow rate in model A was about +1% too high.

Although Reynolds similarity is chosen to generate similar flow patterns, a drawback of this approach is that the sedimentation process is not scalable by Hazen number if the settling velocity is the same in the models and the full-scale device. This can be seen from the fact that model A is operated at a higher surface loading rate than model B, while both are again operated at higher surface loading rates than the full-scale device, see Table 1. However, if the same particle material is used and is not scaled in accordance with the geometric relationship of model A and model B, the settling velocity of a particle with a specific diameter remains constant in both models. Consequently, both models are operated at different Hazen numbers concerning particles with the same diameter, which prevents a direct comparison. To avoid this obstacle, the removal efficiency in this experimental setup is determined for very fine particle classes that approximate the behavior of individual particles (see SI for more information). Since each particle-size corresponds to an individual settling velocity, this results in a set of different Hazen numbers. Assuming that scaling with the Hazen number can be performed for basin types that deviate from the classic rectangular basins, the removal efficiency is expected to be the same for the same numerical value of the Hazen number in both models of the CTD-SF. To test this hypothesis in the framework of this study, the particle-size-specific removal efficiencies by sedimentation are evaluated in models A and B. For the tests, the standard material Millisil W4 was used as particulate matter. The applied measurements and methods are described in section 2.4. Additionally, the determination of the Hazen number requires the settling velocities of the considered particles. These are calculated according to a type I settling behavior and Newton's equation (Bolognesi *et al.* 2012) using the Kaskas equation for the drag coefficient (Goossens 2019), see SI for additional information.

2.3. Investigation of flow pattern similarity with tracer experiments

To control if Reynolds similarity produces similar flow patterns in the given geometry, tracer experiments are carried out in models A and B. Thereby, the tracer is injected into the inlet and measured at the outlet. As stated, the modeling of the CTD-SF in this publication does only include the filter resistance towards the flow, i.e. the effect of the filter resistance on the flow within the preliminary sedimentation stage. Following this concept, the internal flow inside the filter media is not modeled. Since the filter mats are between injection and measurement point, they can therefore cause distortion of the tracer signal and prevent a comparison. A measurement in both models A and B underneath the filter mats was discarded, since the invasive measurement can likewise cause distortion of the tracer signal. Thus, the similarity of flow patterns could only be evaluated for both models without filter mats. However, if the tracer signals indicate similar flow patterns in both models at the same Reynolds number, i.e. at the same ratio of inertial to viscous forces, then it can be assumed that these forces are also governing the flow pattern even when a filter is included.

Dissolved sodium chloride was used as a tracer substance and injected by a peristaltic pump (WATSON, Marlow) into the inlet pipe. Effluent tracer concentration is measured as electric conductivity (TetraCon 925; WTW GmbH, Germany) at the outlet pipe. Time and duration of tracer injection are detected in the inlet by the current increase between two electrodes at a constant voltage supply. Voltage and current are recorded using current/voltage bricklets 2.0 (Tinkerforge GmbH, Germany). Because of Reynolds similarity, models A and B are operating at different time scales. The dependence of time scales and length scales according to Reynolds similarity can be described as follows (Kobus 1984):

$$\frac{t_B}{t_A} = \left(\frac{L_B}{L_A}\right)^2 \tag{4}$$

where t_A (s) is the time scale in model A and t_B (s) is the time scale in model B. L_A and L_B (m) are the length scales of the models A and B, respectively. The duration of tracer injection was therefore adapted to the relationship of Equation (4). Thereby, the duration of the tracer injection in model B is increased by the factor of $(L_B/L_A)^2$ compared to model A. For this purpose, the volume of tracer was increased in model B, while the injection speed of the peristaltic pump was equal in both models, see Table 1. In addition, the occurrence of density currents, i.e. flow patterns occurring due to density differences between tracer solution and water, was taken into account (Adamsson 2004). Therefore, different sodium chloride concentrations (25, 50 and 100 g L^{-1}) were tested on model B. All tracer signals were de-dimensionalized following Levenspiel (2014) to allow comparison of systems operating on different length and time scales. Thereby, the nondimensional

time is represented by θ and the nondimensional concentration by $E(\theta)$. Additional information on de-dimensionalization of tracer signals is given in the SI of this publication.

2.4. Determination of particle-size-specific removal efficiencies

Particles were dosed upstream in the inlet pipe in both models A and B. Millisil W4 quartz sand with a density of 2.65 g cm^{-3} was used for the tests, which is commonly used as a model material for road dust. Assuming that low particle concentrations do not affect settling behavior, a constant flow sediment feeder was not used (Thompson 1969; Weiß & Michelbach 1996). Hence, batch feeding was performed with dry Millisil W4 in increments of roughly 230 ± 29 mg. The particle-size-specific removal efficiency was determined using a combined method of sieving and laser diffraction for models A and B, see Figure 2. Firstly, Millisil W4 was fractionated by dry sieving (AS 200 control, Retsch, Germany) into fractions of 40–63, 63–100, 100–125, 125–160, 160–200 and >200 μm. Dry sieving steps were carried out according to Gelhardt *et al.* (2017). The fractionated masses were collected separately. For the sedimentation test a Standard with a defined composition was compiled from the collected fractions. The composition of the Standard is depicted in Table S1. This Standard was dosed to the inlet of the models. At the end of a sedimentation test, i.e. when the complete standard was dosed to the model, particulate matter that remained in the sedimentation chamber of the system was collected. Note that the filter mats were backwashed after each sedimentation test to avoid the accumulation of particles. The sediment was then fractionated via a subsequent dry sieving step and weighted. Within selected sieving fractions (40–63, 63–100 and 100–125 μm), the particle-size distribution (PSD) in both the standard and the sediment is determined by laser diffraction. For this purpose, samples were drawn from the fractions of the Standard and analyzed after drying for 24 h at 105 °C. In the case of the sediment, due to the small quantity, the complete fractions could be analyzed without taking samples. Each fraction was analyzed separately to reduce uncertainties observed in mixed fraction measurements (Gerlach *et al.* 2003). The particle measurement was carried out in a dry module (Beckman Coulter LS 13 320 with Tornado Dry Powder System, 20 nm to 2,000 μm). In accordance with DIN ISO 13320, the accuracy of the measurement was checked using the certified reference material. The complete procedure, which is shown in Figure 2, was repeated several times depending on the fraction analyzed ($n = 4$–6) for models A and B.

The particle-size-specific removal efficiency η is calculated in the following manner:

$$\eta = \frac{\sum_i \mathrm{PSD}_{i,\mathrm{sediment}} \cdot M_{i,\mathrm{sediment}}}{\sum_i \mathrm{PSD}_{i,\mathrm{standard}} \cdot M_{i,\mathrm{standard}}} \tag{5}$$

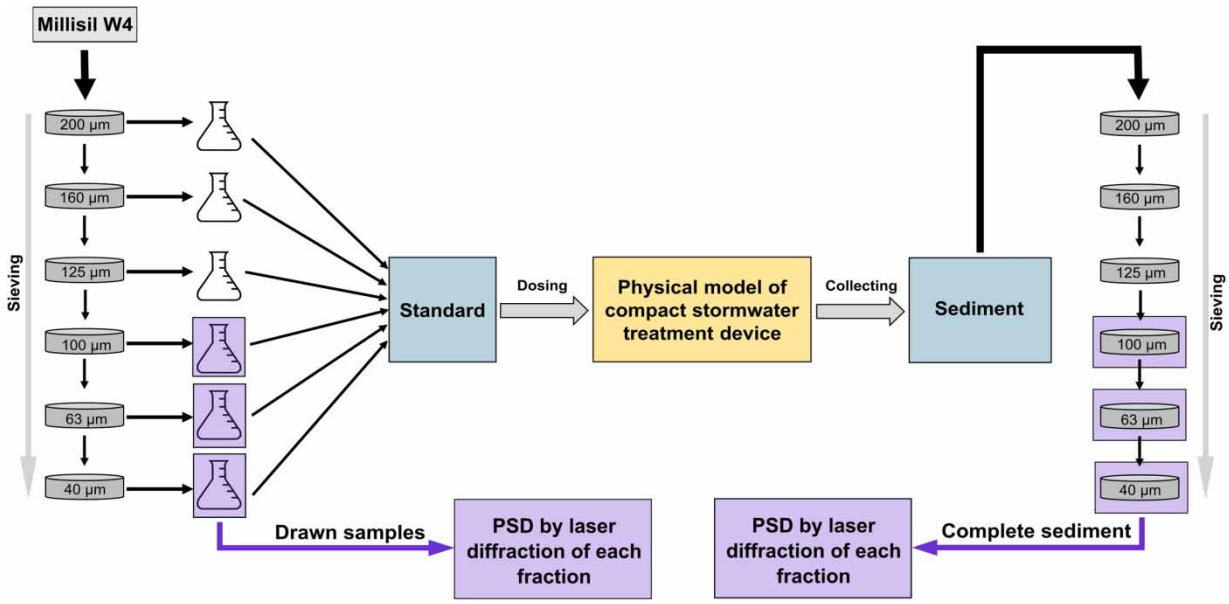

Figure 2 | Sampling and analyzing procedure for determination of particle-size-specific removal efficiency of Millisil W4.

where $PSD_{i,XXX}$ (–) is the PSD of the ith fraction from measurements of *sediment* or *standard* particulate matter. The index i corresponds to the sieving fractions ($i = 40$–63, 63–100, 100–125 µm). $M_{i,\text{sediment}}$ (g) is the mass of the sediment being in the sieving fraction i, while $M_{i,\text{standard}}$ (g) is the mass of the standard which was dosed being in the sieving fraction i. It should be noted that very low mass fractions of about $< 5\%$ in the determined PSDs were discarded for the calculation of Equation (5), since they contribute little to the overall removal efficiency, but at the same time have a high measurement uncertainty. An example is displayed in Figure S5.

2.5. Mathematical model of classical sedimentation theory

A commonly used model for predicting removal efficiencies in settling basins is the model of Hazen (1904) which is also used in the American design recommendations (Fair & Geyer 1954; EPA 1986):

$$\eta = 1 - \left(1 + \frac{1}{n} \cdot \frac{v_s}{q_A}\right)^{-n} \tag{6}$$

where η (–) is the removal efficiency, v_s (m h^{-1}) is the settling velocity, q_A (m h^{-1}) is the surface loading rate and n (–) is a model parameter. According to Hazen (1904), the parameter n corresponds to the degree of mixing inside the settling tank: Thereby, for a parameter of $n = 1$, the removal efficiency corresponds to the performance of a continuously stirred tank reactor (CSTR), while $n \to \infty$ corresponds to the performance of an ideal plug flow (PFR) with no backmixing. The latter one represents the ideal settling device. Deviations from this are caused by backmixing and short-circuiting.

3. RESULTS AND DISCUSSION

3.1. Flow pattern

A visualization of the system with a qualitative flow pattern from numerical simulations is shown in Figure 3. Detailed information on numerical simulations of CTDs combining sedimentation and filtration is given in Stricker *et al.* (2022). Herein, 3D

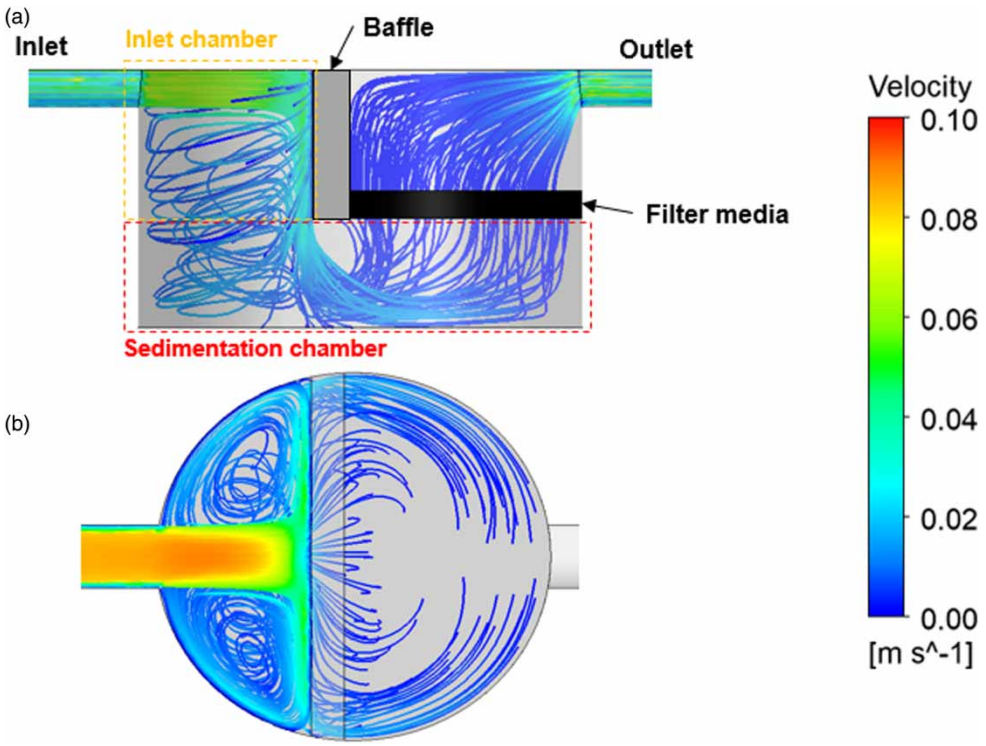

Figure 3 | Qualitative streamlines at a rainfall intensity of 5 L s^{-1} ha^{-1} viewed from (a) cross-section and (b) top in the full-scale compact stormwater treatment device.

simulations were performed at steady-state conditions for a full-scale combined filter-lamella separator using the commercial software ANSYS Fluent 19.1. The filtration stage was represented by a porous media model, which allows the pressure drop to be modeled as a function of the permeability of the filter material. As turbulence model, the standard k-ε model was used. However, within this study numerical simulations are only carried out for visualization of the qualitative flow pattern in the CTD-SF. In Figure 3, it can be seen that the incoming stormwater is deflected by the baffle. Thereby, a downward-directed flow develops along the baffle. The stormwater transported by this flow is then horizontally crossing the sedimentation chamber and passing through the filter media. While a large part of the stormwater reaches the filter in this way, the deflection by the baffle causes vortices to form, especially in the inlet chamber, see Figure 3(b). These vortices continue down to the bottom into the sedimentation chamber and are generated by left- and right-deflected currents.

3.2. Tracer experiments

Tracer experiments were initially conducted at different sodium chloride concentrations of 25, 50 and 100 g L^{-1} on model B. The goal was to find the tracer concentration that would provide the best recovery rate without changing the flow field due to density differences between the tracer solution and the water. The results are depicted in Figure S3 showing that a concentration of 100 g L^{-1} changes the tracer signal, while concentrations of 25 and 50 g L^{-1} produce identical results. In this case, the tracer solution with a concentration of 100 g L^{-1} preferentially follows the flow near the bottom, which is the fastest path to the outlet of the system in this setup (without filter mats). However, with higher concentrations, the recovery rate of the tracer experiments improved from 84 to 94%, for 25 to 50 g L^{-1}, respectively.

Thus, subsequent tracer experiments were carried out with a sodium chloride concentration of 50 g L^{-1}. The tracer signals for models A and B at Reynolds similarity and without filter stages are shown in Figure 4. As expected, a higher peak concentration and a shorter residence time are observed in model A, see Figure 4(a). Here, the differences between model A and B arise from the differences on the time and length scales between the two models. However, the differences disappear when the tracer signals are de-dimensionalized, see Figure 4(b). In this case, it can be concluded that the main flow patterns are similar in both models. Consequently, the similarity of flow patterns can be achieved by operating the models at Reynolds similarity.

3.3. Particle-size-specific removal efficiencies

Figure 5 shows the particle-size-specific removal efficiencies of both models at Reynolds similarity. Obviously, the removal efficiencies in model A are substantially lower than in model B, see Figure 5(a). This observation is in accordance with Reynolds similarity since higher velocities in the small model decrease the removal by sedimentation. For instance, in model A the removal efficiency of a particle of roughly 63 μm is at 40%, while in model B it is at around 60%. Without further

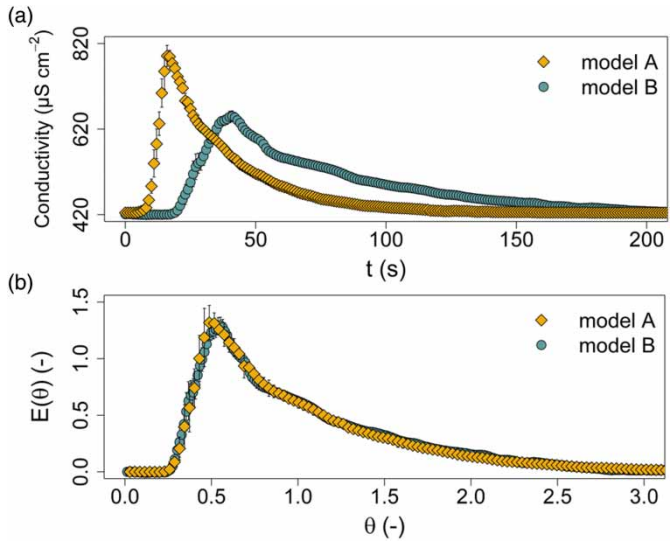

Figure 4 | Tracer signals of models A and B at Reynolds similarity with (a) dimensional and (b) nondimensional parameters.

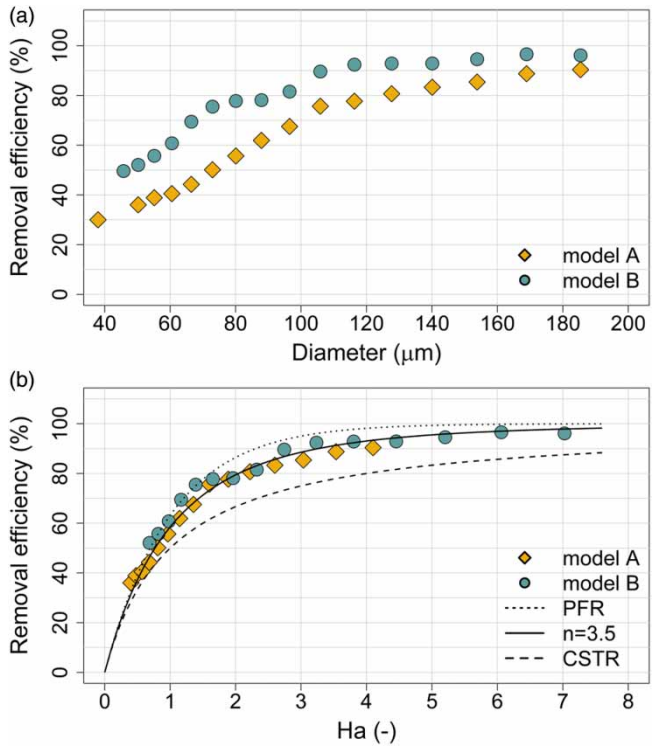

Figure 5 | Removal efficiencies of Millisil W4 in models A and B at Reynolds similarity in (a) dimensional and (b) nondimensional parameters using Hazen number.

investigation by other nondimensional numbers, the results can hardly be extrapolated to the full-scale of the original. In Figure 5(b), the Hazen number is used as a nondimensional group and plotted against the corresponding removal efficiencies. Herein, the removal efficiencies of model A and B fall on one line when the Hazen number is applied. From this observation, several information can be drawn: Firstly, similarity concerning removal efficiencies can be achieved between models A and B by applying the Hazen number as a nondimensional group. Thereby, the internal flow of the device under investigation does not necessarily need to match with the theory of uniform flow in a rectangular basin, see Figure 3. These results agree with those of Thompson (1969), who identified that the Hazen number produces similarity between two geometrically similar model tanks of different scales, while the flow patterns deviated from the ideal. Nevertheless, in the present study, it is noticeable that the removal efficiencies observed in model A lag somewhat behind those of model B to some smaller extent, see Figure 5(b). This may be a result of the uncertainties in the proposed sampling and analyzing procedure, see Figure 2. Additionally, it is possible that it is caused by enhanced scouring in model A, i.e. higher shear stress impacting the removal efficiency. However, this assumption cannot be conclusively evaluated within the scope of this study. Therefore, transferring the results to the full-scale could lead to an underestimation of the removal efficiencies in the full-scale device. Further investigations on models with different length scales or different rainfall intensities should give a deeper insight on this topic. In addition, the removal efficiencies could be underestimated if the flow conditions in the inlet pipe of the full-scale device change to laminar flow, since the flow was kept turbulent in the experiments. This is only expected for small rain fall intensities ≤ 1 L s^{-1} ha^{-1}.

To investigate the applicability of classical theoretical models, the removal efficiencies are calculated according to Equation (6) assuming a CSTR and PFR basin. Herein, the CSTR assumption significantly underestimates the removal efficiencies of the sedimentation chamber, while the assumption of an ideal PFR tends to overestimate the removal efficiencies. A best fit for the classical mathematical model was achieved for $n = 3.5$, which corresponds to three and a half CSTRs in series, see Figure 5(b). The results coincide with the investigations of Liu & Sansalone (2019) who found that the classical CSTR model of Hazen underestimates removal efficiencies in a hydrodynamic separator for stormwater treatment. Testing different CTDs and comparing them to the classical Hazen model, Boogaard *et al.* (2015) suggest that deviations from the

mathematical model can be referred to the effectively used settling area. Quantitatively, the removal efficiency of the sedimentation chamber of the CTD-SF in this study is in the order of magnitude of the removal efficiencies determined by Boogaard *et al.* (2015). Generally, the results match with the observation of Li & Sansalone (2021), who determined that the Hazen number is a relatively robust parameter for scaling removal efficiencies in clarification basins. However, within their results, this did not imply that the predictions of classical theoretical models were correct. This reflects the results of this study since the Hazen number is able to achieve similarity. Nevertheless, the classical theoretical model needs calibration with respect to the characteristics of device.

3.4. Site-specific prediction of the filter load on the full-scale device

Based on the calibrated mathematical model, the filter load can be predicted for a range of surface loading rates and settling velocities. By using the dimensionless numbers (Hazen number and removal efficiency), the relationship in Figure 5(b) can be applied regardless of the sediment material. Therefore, the proposed relationship, which is described by the calibrated model, can be applied not only to the full-scale device but also to other catchment sites. However, it is a prerequisite that the settling velocity distribution (SVD) of the particles from the catchment site of interest is known. This can be calculated from the PSD in road runoff using sedimentation models that are able to predict settling velocities with acceptable errors (Rommel *et al.* 2020). It should be noted that these models generally assume a type I settling behavior, i.e. low volume concentrations of particles. Alternatively, the SVDs can be measured directly. However, the experimental setup has a strong influence on the results. In this study, the PSD of Millisil W4 is used as an example, which serves as a model material for a rather fine PSD in road runoff, see Figure S4. The PSD of Millisil W4 may be replaced by a PSD of particulate matter from a specific catchment site, so that the CTD-SF can be sized with respect to the local boundary conditions. In this study, the SVD is calculated according to Equations (S1), (S2), and (S3) based on the PSD of Millisil W4. From this, the filter load under different hydraulic loading conditions can be predicted, which is an important design parameter for the service life of the filter. Calculations are carried out for the full-scale CTD-SF at rainfall intensities ranging from 2.5 to 15 L s^{-1} ha^{-1} in steps of 2.5 L s^{-1} ha^{-1}, i.e. at surface loading rates of 2, 4, 6, 8, 10 and 12 m h^{-1}. For each fraction of the SVD, six Hazen numbers can be calculated according to the six surface loading rates. Applying the calibrated mathematical model ($n = 3.5$) from Figure 5(b), the removal efficiency by sedimentation can be predicted for each Hazen number. Consequently, the filter load, i.e. the share of particulate matter which is loaded to the filter can be estimated. In Figure 6, the percentage of particulate matter being loaded to the filter and the percentage that settles in the sedimentation stage are illustrated at different surface loading rates.

Evidently, the percentage of particulate matter being loaded to the filter increases from 20 to 40% with an increasing surface loading rate. For instance, assuming a surface loading rate of 4 m h^{-1}, which coincides with the German average rainfall intensity of 5 L s^{-1} ha^{-1}, the filter inside the investigated CTD-SF is loaded by roughly one-fourth of the incoming mass of particulate matter. In addition to the filter load, the PSD in the influent of the filter is estimated for the full-scale CTD-SF at different surface loading rates, see Figure 7. As expected, the composition of particulate matter in the influent of the

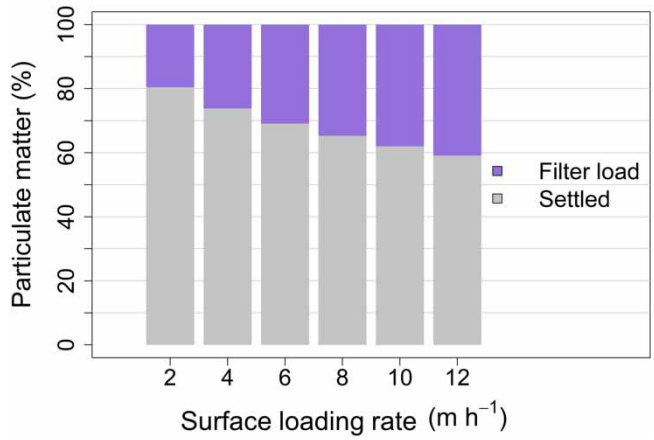

Figure 6 | Percentage of particulate matter being removed by sedimentation and loaded to the filter at different surface loading rates for Millisil W4 in the full-scale device.

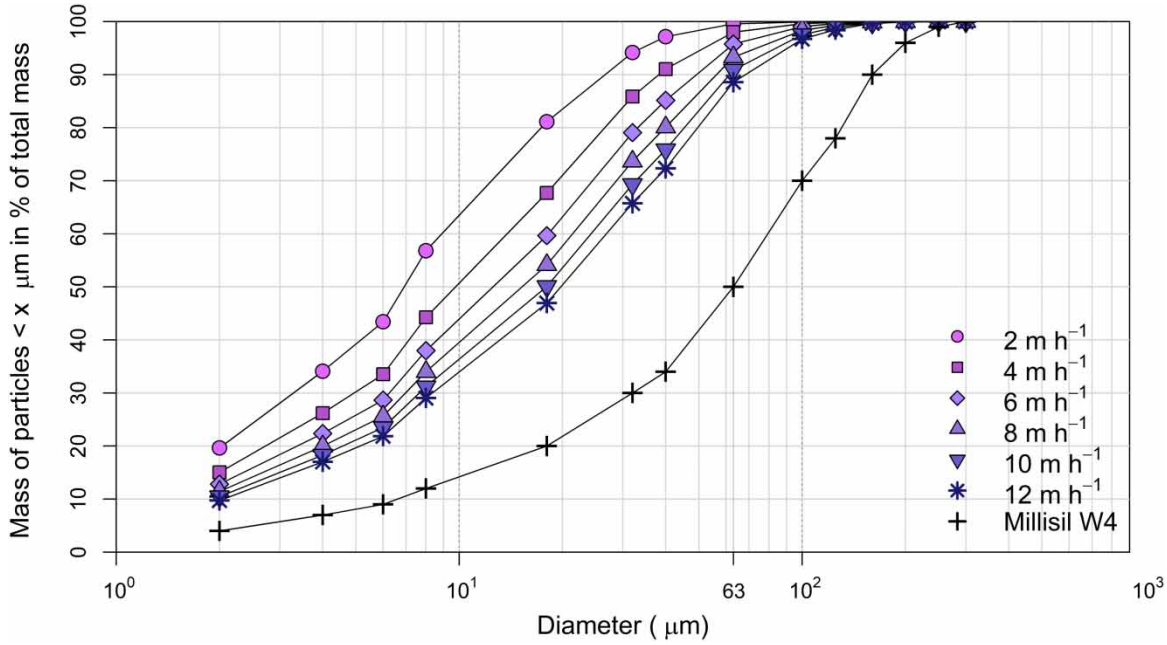

Figure 7 | Particle-size distribution in the influent of the filter at different surface loading rates in the full-scale device and particle-size distribution of Millisil W4.

filter becomes coarser as the surface loading rate increases. However, even at a high surface loading rate of 12 m h^{-1}, the majority of particulate matter can still be attributed to the spectrum of particles with a diameter ≤63 µm. Thereby, the d_{63} is approximately at 88% and at 99% for surface loading rates of 12 and 2 m h^{-1}, respectively. Note that the results displayed in Figures 6 and 7 will change if the PSD and particle density differ greatly from the properties of Millisil W4.

The results in Figures 6 and 7 are relevant to properly dimensioning CTD-SFs concerning catchment area, filter area and filter structure. Thereby, the filter stage in CTD-SFs is only partly loaded by particulate matter in the road runoff since a preliminary sedimentation retains larger particles. Additionally, it can be expected that particulate matter loaded to the filter stage in CTD-SFs is rather fine compared to particulate matter in untreated road runoff. Since both particle size and the mass of particulate matter loaded to the filter are important parameters that affect the lifetime of a filter stage, the sedimentation stage is likely to slow down the process of filter clogging. To what extent, however, also depends on the properties of the filter material (Kandra *et al.* 2015). Consequently, studies investigating the lifetime of a CTD-SF as a result of mechanical clogging should consider the loading conditions and the properties of the filter material.

4. CONCLUSION

In the present study, a compact stormwater treatment device combining sedimentation and filtration is investigated by physical hydraulic modeling. Verification of scaling laws is carried out by comparing the results of two geometrically similar small-scale models at different length scales. Thereby, tracer experiments confirm that Reynolds number similarity produces similar flow patterns in both models. Moreover, the Hazen number successfully creates the similarity of particle-size-specific removal efficiencies in the sedimentation chamber even when the flow pattern deviates from the theoretical concept of a uniform flow in a rectangular basin. However, models of classical sedimentation theory cannot be used without calibration and may otherwise incorrectly predict removal efficiencies in compact stormwater treatment devices. Upscaling to the full-scale shows that, on average, the filter stage is only loaded with one-fourth of the total particulate matter in the inlet of the device. Furthermore, even at rainfall intensities of 15 L s^{-1} ha^{-1}, about 88% of the particles in the influent of the filter still belong to the spectrum of particles ≤63 µm. These results are obtained assuming a PSD of Millisil W4 and a type I settling behavior. Other values may result under different boundary conditions. However, it becomes clear that sedimentation upstream of a filter is of relevant importance in CTDs. Overall, physical hydraulic modeling was able to provide information on the functionality of CTDs with combined sedimentation and filtration without the effort of full-scale measurements. Future investigations may extend the

range of volume flows tested in this study. Additionally, the information generated on small-scale models may be used to complement numerical modeling studies.

ACKNOWLEDGEMENTS

This work was supported by the Ministry for Culture and Science of the State of North-Rhine Westphalia (NRW, Germany) through the joint project 'Future Water' (project number: 321-8.03-215-116439).

DATA AVAILABILITY STATEMENT

All relevant data are included in the paper or its Supplementary Information.

CONFLICT OF INTEREST

The authors declare there is no conflict.

REFERENCES

Adamsson, Å. 2004 *Three-Dimensional Simulation and Physical Modeling of Flows in Detention Tanks: Studies of Flow Pattern, Residence Time and Sedimentation*, Göteborg, Sweden.

Bolognesi, A., Ciccarello, A., Maglionico, M., Kim, J.-Y., Artina, S. & Sansalone, J. 2012 Can surface overflow rate predict particulate matter load capture for common urban drainage appurtenances? *Journal of Environmental Engineering* **138** (7), 723–733.

Boogaard, F. C., van de Ven, F., Langeveld, J. G., Kluck, J. & van de Giesen, N. 2015 Removal efficiency of storm water treatment techniques: standardized full scale laboratory testing. *Urban Water Journal* **14** (3), 255–262.

Camp, T. R. 1946 Sedimentation and the design of settling tanks. *Transactions of the American Society of Civil Engineers* **111** (1), 895–936.

Clements, M. S., Price, G. A., McConnachie, G. L. & Thompson, D. M. 1969 Technical note. scaling laws for continuous flow sedimentation in rectangular tanks: discussion. *Proceedings of the Institution of Civil Engineers* **46** (3), 387–393.

DIN ISO 13320 2020 *Partikelgrößenanalyse – Laserbeugungsverfahren*.

Dufresne, M., Dewals, B. J., Erpicum, S., Archambeau, P. & Pirotten, M. 2010 Experimental investigation of flow pattern and sediment deposition in rectangular shallow reservoirs. *International Journal of Sediment Research* **25** (3), 258–270.

DWA and BWK 2020 *Arbeitsblatt DWA-A 102-2/BWK-A 3-2: Grundsätze zur Bewirtschaftung und Behandlung von Regenwetterabflüssen zur Einleitung in Oberflächengewässer - Teil 2: Emissionsbezogene Bewertungen und Regelungen (Worksheet DWA-A 102-2/BWK-A 3-2 Guidelines for the Management and Treatment of Stormwater Runoff for Discharge Into Surface Waters - Part 2: Emission Related Assessments and Regulations)*, 1st edn. Hennef, Germany.

Emori, R. I. & Schuring, D. J. 1977 *Scale Models in Engineering: Fundamentals and Applications*. Elsevier Science, Burlington.

EPA 1986 *Methodology for Analysis of Detention Basins for Control of Urban Runoff Quality EPA440/5-87-001*.

Fair, G. M. & Geyer, J. C. 1954 *Water Supply and Waste Water Disposal*. John Wiley and Sons, New York.

Fletcher, T. D., Shuster, W., Hunt, W. F., Ashley, R., Butler, D., Arthur, S., Trowsdale, S., Barraud, S., Semadeni-Davies, A., Bertrand-Krajewski, J.-L., Mikkelsen, P. S., Rivard, G., Uhl, M., Dagenais, D. & Viklander, M. 2015 SUDS, LID, BMPs, WSUD and more – the evolution and application of terminology surrounding urban drainage. *Urban Water Journal* **12** (7), 525–542.

Gelhardt, L., Huber, M. & Welker, A. 2017 Development of a laboratory method for the comparison of settling processes of road-deposited sediments with artificial test material. *Water, Air and Soil Pollution* **228** (12), Article 467.

Gerlach, R. W., Nocerino, J. M., Ramsey, C. A. & Venner, B. C. 2003 Gy sampling theory in environmental studies. *Analytica Chimica Acta* **490** (1–2), 159–168.

Goossens, W. R. 2019 Review of the empirical correlations for the drag coefficient of rigid spheres. *Powder Technology* **352**, 350–359.

Grüning, H. & Schmitz, T. 2018 Teil 2: Systeme zur technischen Regenwasserfiltration: Kennwerte und Bemessung. (Part 2: technical rainwater filtration: key figures and dimensioning). *GWF-Wasser/Abwasser* **159** (3), 63–69.

Hazen, A. 1904 On sedimentation. *Transactions of the American Society of Civil Engineers* **53** (2), 45–71.

Herr, C. & Sansalone, J. J. 2015 In situ volumetric filtration physical model to separate particulate matter from stormwater. *Journal of Environmental Engineering* **141** (9), 4015017.

Huber, M., Welker, A. & Helmreich, B. 2016 Critical review of heavy metal pollution of traffic area runoff: occurrence, influencing factors, and partitioning. *The Science of the Total Environment* **541**, 895–919.

Kandra, H., McCarthy, D. & Deletic, A. 2015 Assessment of the impact of stormwater characteristics on clogging in stormwater filters. *Water Resources Management* **29** (4), 1031–1048.

Kawamura, S. 1981 Hydraulic scale-model simulation of the sedimentation process. *Journal-American Water Works Association* **73** (7), 372–379.

Kobus, H. 1984 *Wasserbauliches Versuchswesen, Schriftenreihe des Deutschen Verbandes für Wasserwirtschaft und Kulturbau e*. Vol. 39. Parey, Hamburg.

Langeveld, J. G., Liefting, H. J. & Boogaard, F. C. 2012 Uncertainties of stormwater characteristics and removal rates of stormwater treatment facilities: implications for stormwater handling. *Water Research* **46** (20), 6868–6880.

Levenspiel, O. 2014 *Tracer Technology: Modeling the Flow of Fluids*. Softcover reprint of the hardcover 1st edition 2012, Fluid mechanics and its applications, Vol. 96. Springer, New York, NY, Dordrecht, Heidelberg.

Li, H. & Sansalone, J. 2021 A CFD-ML augmented alternative to residence time for clarification basin scaling and design. *Water Research* **209**, 117965.

Lieske, C., Leutnant, D. & Uhl, M. 2021 Assessing the TSS removal efficiency of decentralized stormwater treatment systems by long-term In-Situ monitoring. *Water* **13** (7), 908.

Liu, H. & Sansalone, J. 2019 CFD and physical models of PM separation for urban drainage hydrodynamic unit operations. *Water Research* **154**, 258–266.

Maniquiz-Redillas, M. & Kim, L.-H. 2014 Fractionation of heavy metals in runoff and discharge of a stormwater management system and its implications for treatment. *Journal of Environmental Sciences* **26** (6), 1214–1222.

Neupert, J. W., Lau, P., Venghaus, D. & Barjenbruch, M. 2021 Development of a new testing approach for decentralised technical sustainable drainage systems. *Water* **13** (5), 722.

Rommel, S. H., Gelhardt, L., Welker, A. & Helmreich, B. 2020 Settling of road-deposited sediment: influence of particle density, shape, low temperatures, and deicing salt. *Water* **12** (11), 3126.

Sekimoto, K., 2008 Scaling laws for sedimentation process in water flow-driven sedimentation tanks. In: *Progress in Scale Modeling* (Saito, K., ed.). Springer Netherlands, Dordrecht, pp. 379–390.

Sommer, H. 2015 *Dezentrale Behandlung von Straßenabflüssen: Übersicht verfügbarer Anlagen*. (Decentralized treatment of street runoff: Overview of available facilities). Available from: http://www.sieker.de/daten/download/DSWT/Broschüre_Dezentrale_Regenwasserbehandlung.pdf (accessed 1 February 2023).

Spelman, D. & Sansalone, J. J. 2018 Is the treatment response of manufactured BMPs to urban drainage PM loads portable? *Journal of Environmental Engineering* **144** (4), 1–10.

Stovin, V. R. & Saul, A. J. 1994 Sedimentation in storage tank structures. *Water Science and Technology* **29** (1–2), 363–372.

Stricker, M., Littfinski, T., Heinz, E., Pecher, K. H., Lübken, M., Grüning, H. & Wichern, M. 2022 Design-oriented evaluation of the hydrodynamics in a full-scale combined filter-lamella separator for urban stormwater treatment. *Water Science and Technology* **85** (10), 2854–2868.

Takamatsu, M., Barrett, M. & Charbeneau, R. J. 2010 Hydraulic model for sedimentation in storm-water detention basins. *Journal of Environmental Engineering* **136** (5), 527–534.

Thompson, D. M. 1969 Technical note. Scaling laws for continuous flow sedimentation in rectangular tanks. *Proceedings of the Institution of Civil Engineers* **43** (3), 453–461.

Weiß, G. J. 1997 Vortex separator: proposal of a dimensioning method. *Water Science and Technology* **36** (8–9), 201–206.

Weiß, G. J. & Michelbach, S. 1996 Vortex separator: dimensionless properties and calculation of annual separation efficiencies. *Water Science and Technology* **33** (9), 277–284.

Wichern, M., Pecher, K. H., Helmreich, B., Vesting, A., Heinz, E., Giga, A., Wolke, M., Huber, M. & Li, Y. 2017 *Reduktion von Kohlenwasserstoffen und anderen organischen Spurenstoffen durch ein dezentrales Behandlungssystem für Verkehrsflächenabflüsse (Reduction of Hydrocarbons and Other Organic Trace Substances in A Decentralized Treatment System for Road Runoff): Award no. 08/058.2*. Report for the Ministry for Environment, Agriculture, Conservation and Consumer Protection of the State of North Rhine-Westphalia (MULNV), Germany.

First received 17 November 2022; accepted in revised form 20 January 2023. Available online 1 February 2023